Ultra Scientist Vol. 26(1)B, 61-90 (2014).

Application of ASTER imageries and mathematical evaluation method (MEM) in detecting spatial distribution relationship of cyanobacteria and iron contamination in biological soil crust, Chadormalu area, central Iran

A. MOGHTADERI*†

(Acceptance Date 22nd February, 2014)

Abstract

Iron is an essential element for almost all living species. Previous studies demonstrated that both the growth rate and concentration of chlorophyll *a* in cultures of cyanobacteria were limited by insufficient Fe concentrations. The cyanobacteria biological soil crust in desert where most rain falls seasons are dominated by filamentous species are well adapted for primary colonization of arid environments due to their extraordinary ability to survive desiccation and extreme temperature, high pH and salinity. Satellite imageries are widely used to map geological and environmental features at different scales. To date, little research has been done to spectrally examine biological soil crusts or map them using remote sensing. Recent researches demonstrated that ASTER visible- near infrared scanner systems can be used successfully to map iron ores and cyanobacteria soil crust. In this study Mathematical Evaluation Method (MEM) performed on ASTER imagery data, firstly. This research demonstrates cyanobacteria growth –iron contamination relationships by remote sensing techniques at the Chadormalu desert, Yazd Province, Iran. In other words, this study illustrates directional relationship of spatial distribution between cyanobacteria soil crust and major iron ores contamination at this mining area, probably related to cyanobacteria physiology. The MEM method, despite being approximate is suitable in detecting iron contamination in inaccessible remote areas on earth or may be useful in astrobiological studies, especially, in Mars biological explorations.

Key words: Iron contamination, Cyanobacteria, ASTER, MEM, Fe concentration, Chadormalu.

*****Corresponding author. E-mail address: a_moghtaderi@pnu.ac.ir, or moghtaderiarsia@gmail.com

1. Introduction

Iron is an essential element for almost all living species[1]. With the exception of some strains of *lactobacillus*[2] and *Borrelia burgdorferi*[3] iron is a fundamental element for all bacteria[4]; so that previous studies[5,6], demonstrated that both the growth rate and concentration of chlorophyll *a* in cultures of cyanobacteria were limited by insufficient Fe concentrations (<10µM). That is growth of cyanobacteria under conditions of iron deficiency leads to changes in cellular physiology and biochemistry[7]; in other words decreases in cellular pigment levels, protein synthesis, and variations in electron transport components are commonly reported for cyanobacteria grown in iron-deficient conditions[8,9]. Webb *et al*.[4] indicated that *idA* protein may make an excellent marker for Fe stress in open ocean cyanobacterial field populations. According to Berman- Frank *et al*.[10] as increase in iron concentrations in the growth media of cyanobacteria (e.g. *Trichodesmium, Cyanothece, Anabena)* cultures resulted in an increase for the photosynthetic activity and N-fixation.

The cyanobacteria biological soil crust (CSC) in desert where most rain falls seasons are dominated by filamentous species such as *Microcoleous* and smaller genera such as *Scytonema, Nostoc,* and *Schizothrix*[11] are well adapted for primary colonization of arid environments due to their extraordinary ability to survive desiccation and extreme temperature (up to 70°C), high pH and salinity[12]. These organisms contribute to soil stability[13] soil build up[14], soil fertility[15] and to the soil water regime[16].

Satellite imageries are widely used to map geological and environmental features at different scales[17-20]. To date, little research has been done to spectrally examine biological soil crusts or map those using remote sensing[21]. Karnieli *et al*.[22] have shown that spectral reflectance values can be measured during wet seasons and O' Neill[23], Karnieli and Sarafis[24], Tromp and Steenis[25] and Zombre *et al*.[26], presented spectral curves of cyanobacteria crust. Moghtaderi *et al*.[17] analyzed systematically the spectral features of the cyanobacteria crust through the atmospheric windows available to spectral remote sensing instruments (*i.e.* Visible Near Infrared (VNIR), under dry conditions).

The ability of Visible to Near infrared (VNIR) scanner systems to map gossans, rich in iron and associated with weathered sulfide occurrence, as well as regolith characterization is perhaps the most important current applications of this new technology[27]. Heavy metal contamination of soil mostly results from anthropogenic influences on the physical and chemical characteristics of soil ecosystems. ASTER visible- near infrared and short-wave infrared scanner systems can be used successfully to map iron ores[28, 29].

Detecting and mapping a variety of surface features using image data can be obtained by a number of different techniques (e. g. minimum noise fraction (MNF) transform, matched filtering, spectral linear mixture, band ratio, etc.[17,30,31-33]). Conradsen and Harpoth[30] used Landsat MSS band ratio (4/5, 5/7, 6/7) for detection and reconnaissance mapping of iron oxide at central east Greenland. These researchers detected limonitic rocks in pink to

orange color (false color composite). Abdelsalam *et al*.[31] generated clay and Fe alteration index map by density slicing for Landsat TM band ratio 5/7 and 3/1, respectively. Landsat 5/7- 4/5- 3/1 TM images characteristically depict small (tens of pixels) gossans in blue and the more extensive alteration zones in pinkish purple. Moghtaderi *et al*.[32,33], using MNF transform and Mathematical Evaluation Method (MEM) on ASTER images demonstrated the capability of ASTER data in the detecting alteration minerals in the Chadormalu iron ore deposit, central Iran. The output of applying MEM is a gray scale image, in which the Digital Number (DN) values match the percent of the alteration mineral present. Moghtaderi *et al*.[17] proposed that the MEM method despite being approximate is suitable in detecting microorganisms (*i. e*. cyanobacteria) in inaccessible areas such as extraterrestrial planet surfaces or remote areas on Earth, especially in extreme dry conditions. As a result, the potential of ASTER imagery data for spectral analysis in geological and environmental investigations is a well-established fact now.

The main purpose of this research is to demonstrate cyanobacteria growth –iron contamination relationships by remote sensing techniques and ground controls at the Chadormalu desert, Yazd Province, Iran. In other words, this study illustrates relationship of spatial distribution between cyanobacteria soil crust and major iron ores contamination at this mining area. This research is an attempt to show remote sensing ability in detecting relations between cyanobacteria soil crust area size, and iron contamination extension.

2. Material and Methods

2.1. Meteoroidal and geological background:

The Chadormalu area (including the northern desert) is located in the Bafq metallogenic province in central Iran, about 115 km southeast of Yazd city (55° 15' - 55° 45' E, 32° 15' -32° 25' N) (Fig 1a, b). The extreme aridity of the Chadormalu desert is due to the Zagros and Alborz mountain ranges to the west and north respectively which prohibit wet (or rainy) weather from reaching this area. Also, the salt deserts (kavir) of Bafq and Saqand occupy west and north of the Bafq region. The average annual rainfall is 55.7 mm and it only rains in the winter and early spring (January-April). Average minimum daily temperatures ranges from -9.6°C in January to 25°C in May, while average maximum daily temperature ranges between 18°C and 45°C in January and July, respectively.

2.2. Spectral characteristics of cyanobacteria and major iron ores:

In semi arid and arid areas the spectral reflectance curves (SRC) of surface materials may be used directly to infer natural surface features, like the biological soil crust and iron ore minerals in this research[23,34,35,36,37,38]. Laboratory reflectance spectra are accessible over the Internet from the USGS (United States Geological Survey) digital spectral library *(http://speclab.cr.usgs.gov/spectral.lib04/spectral-lib.desc+plots.html)*. These sites provide data on minerals, rocks, vegetation and soils but there are no data on microphytic (e.g. cyanobacteria) crusts. For this study the most appropriate spectral curve selection criterion is the spectra of dry cyanobacteria crust proposed

by Karnieli and Sarafis[24] (Fig. 2a), because it is measured from *Microcoleous Vaginatus* and *Nostoc* which, with *Schizothrix, Calothrix, Chroococcidiopsis and Phorimidium* constitutes the most common cyanobacteria (genus) found in the deserts of the world[39,40]. Sharp fluctuations in the reflectance spectral curves for cyanobacteria were used to determine the best ASTER bands (3, 2, 1 bands) for the detection of cyanobacteria ('i.e. *M. vaginatus* and *Nostoc*) (Fig 2a and Table. 2). The reflectance curves give useful diagnostic information on the elemental and mineralogical composition[41].

The spectra (colors) of minerals in the VNIR are, to a large extent determined by their transition (e. g. Fe) and rare earth element concentrations[41]. Because iron, in the ferric and sometimes the ferrous state is usually the only element sufficiently abundant at the surface to affect the spectrum, its presence or absence usually determines the VNIR spectrum (i.e. most rocks and soils are reddish or grayscale)[42]. Figure 3(a, b) shows reflectance spectra of two ferric oxides (hematite and magnetite) and a ferric hydroxide (goethite) in the 0.4- 2.5 μm region[19,43], clay- to-silt – sized particles (< 45 μm).

In this study, the best spectral curve selection criterion is the particle size of the minerals. The chosen range of the particles size is < 45 μm, which offers comprehensive information about variations in the reflected characteristics of the major iron ore minerals. It must be noted that, hematite and magnetite do not have any sharp fluctuations with particle size between 75- 500 μm (especially, 125-500 μm). According to Vincent[44] reflectance of iron minerals is generally lower for large particle sizes because volume reflectance dominates through most of this wavelength region (0.4- 2.5 μm). Also, this author infers that, pure magnetite is dark and almost featureless in the entire 0.4- 2.5 μm region like most metals. Thus, according to Singer[43], because a single homogenous geologic material is ruled out on spectral grounds as an important dark region component, multiple-component surface should be considered. The simplest such surface would consist of discrete exposures of two materials (*i.e*. magnetite 50%- goethite 50%, < 45 μm). Again, the pure magnetite spectrum is relatively featureless with a slight positive slope (Fig. 3b). Therefore, the additive combinations were calculated based on real coverage by the two end-member components (magnetite and goethite). Clearly an additive situation such as this is inadequate to explain the spectral reflectance of the dark materials. The weighted average of two positively sloping spectra will always have an intermediate positive slope[43]. In this research, field studies and XRD analyses show magnetite-hematite-goethite mixtures at most sampling stations.

The best ASTER bands (3, 2, 1 bands) were selected for detection of hematite and magnetite- goethite (Fig. 3 and Table. 3). In Fig. 2b-f spectral reflectance curves of soil minerals with grain sizes between 150-500 and ≤ 10 μm are displayed. Although these curves may overlap with spectra of wet cyanobacteria crust, examining the spectral reflectance curves of magnetite, hematite and goethite indicate that no such overlaps occur in this study (dry condition).

2.3. ASTER image processing and methodology:

ASTER Image processing was carried

out on the 321 ASTER bands according to Moghtaderi *et al.*[17] in 6 steps. The degree of the proximity of the input DN (Digital Number) values to the hematite, magnetite-goethite (50%-50%) and cyanobacteria reflectance values (Table 2&3) were calculated using the MEM formula proposed by Moghtaderi *et al.*[32]. The output of applying MEM is a gray scale image, in which the DN values correlate with the percentage of the major Fe- minerals (*i.e. hematite, magnetite and goethite*) and Cyanobacteria present. The iron minerals and cyanobacteria components, which are present in the greatest amount, are shown with brighter pixels; these pixels indicate a greater (or major) amount of these features (Fig. 4a-c). The human eye responds more readily to rainbow color than gray scale, so the MEM is presented as a pseudocoloured image in rainbow colors (Fig. 5a-c). Dark and pale pink colors correspond to major amounts of the iron minerals and cyanobacteria, while, green, yellow, cyan, and blue colors represent minor amounts and trace amounts are represented in dark red color.

3. Results

3.1. Image interpretation

MEM (bands 3, 2, 1) shows white and gray pixels or high (major) to low (minor) amount of cyanobacteria (Fig. 4a) in the Chadormalu desert. Elsewhere in the area, White and gray pixels are interpreted to represent thick soil cover (Fig. 7a-c) and black pixels represent thin soil cover (Fig. 7 d, e). At Chadormalu iron mine (Fig 4a and Fig. 7f) there are no white or gray pixels. According to Belnap[45], just as plants increase or decrease with livestock grazing, many biological soil crust components (‘e.g. cyanobacteria) are good indicators of *a lack of* physical disturbance, such as by livestock, human foot traffic, motorized vehicles and mining activity (e.g. Fig. 4a and Fig. 7g). Thus, the black pixels in this area are taken to indicate the degree of disturbance in the area caused by mining.

The iron mineral contents using MEM method are illustrated in figure 4b, c. Hematite and magnetite-goethite are shown in white and gray scale pixels, clearly. The MEM method detected Fe-minerals in chadormalu plain (white and gray pixels~ major and minor amounts) and country rocks (black pixels~ trace amounts); meanwhile, black pixels at mining area can be related to iron ore size (i. e. > 45μm). In this area iron mineral contamination can be seen at sampling station no.17 (magnetite-goethite gouge in mine floor), iron storage bonkers and ore processing factory roofs (Fig. 5d, square area). Ground control revealed that iron minerals are dust size (<45 μm) (Fig. 8b, c and Fig. 9 a, i, j). Pseudocoloured image presentations in rainbow colors (Fig. 5a-c) clearly illustrate relationship of spatial distribution between cyanobacteria soil crust (Fig. 5a) and major iron ores contamination (5b, c).

3.2. Ground control :

3.2.1. Field study :

Field study (ground control) was carried out in late April (18-24 April) in dry conditions, thus dry crust SRC was performed on the ASTER image data. Before performing SRC the metrological data was checked to make sure that there was no rainfall in the days preceding data capture.

As a first step 14 and 17(Fig. 8a-y and 7a-h) sampling stations were selected by the authors in white, gray and black pixels for CSC (Fig 5d) and iron ore contamination (Fig. 5e), respectively. Their coordinates were determined from the georeferenced ASTER data using ENVI 4.7 SP1 (Cursor location/ value window) (Fig. 5d, e; Table 4 and Table 5). The data is orthocorrected, georeferenced and processed by AGARSS Ltd Company, Australia (to an accuracy of ± 45m~ 3 pixels). The selection of sampling stations was done on areas with high density of white and gray pixels (major and minor amounts). In other words, the selection of soil sampling stations was carried out in a way to decrease the soil sampling errors. In the field, each sampling station was verified by GPS instrument (*Garmin Oregon 550*). However, the horizontal error of the instrument is about 5-10m; hence soil sampling is an approximation within a $15m^2$ domain (soil sampling was carried out on thick soil covers).

For cyanobacteria culturing, at each station, soil was picked up (3cm thick) and kept in a plastic bags before being transported (in darkness, 25°C) within few days with no apparent loss of viability. Castenholz[46] protocol was followed for soil sample preparation. Hematite, magnetite and goethite were detected both in the field and by XRD analysis (instrumental characteristics: PW 1800 Philips, Nickel filter and Cu cathodic lamp). XRD analysis revealed that hematite, magnetite and goethite constitute the major phases (Fig. 10a-q).

3.2.2. Culturing, isolation and purification:

In the laboratory, BG-11 media as described by Hughes *et al.*[47] and modified by Allen[48] was used as culture media. After soil solution preparation in deionized distilled water, a two stage serial dilution was performed on the (original) solution. The final soil solutions (final types) were cultured in the solid media (BG-11). The cultures were incubated in a light-dark cycle with a 14-h light period and a 10 dark period for one to two weeks. The temperature of incubation was 20-30°C or room temperature[46, 49,50,51].

3.2.2. Microbiology laboratory studies:

According to Moghtaderi *et al.*[17], the cyanophytes in fully propagated colonies were identified in the solid BG-11 culture media after 1 to 2 weeks. Then, the cultures were examined by a phase-contrast microscope to determine genus and species. They mostly included: *Microcoleous vaginatus*, *Nostoc.sp*, *Microcystis.sp*, *Ocillatoria.sp*, *Chroococcuss. sp* and *Chroococcidiopsis* (Fig. 6a-f). They were found to correspond with the white pixels, especially; sampling stations 1, 2, 4, 6 and 8 (Fig 5d).

4. Discussion and Conclusion

Cyanobacterial Fe requirements are higher than those of eukaryotic algae. These high requirements are commonly attributed to cyanobacterial evolution, since the availability of iron would have been significantly higher in the anaerobic conditions under which these organisms evolved[52]. However, the higher iron requirements of cyanobacteria relative to eukaryotic plankton may also be attributed to reduced amounts of iron-poor structural material in the cyanobacteria, which would lead to a proportional increase in the cellular iron requirements[53].

Table 1. Performance parameters for the ASTER radiometer view (modified from Rowan and Mars, [70], After Fujisada, [69]).

ASTER baseline performance requirements						
System	Band number	Spectral Range (μM)	Radiometric resolution	Absolute Accuracy (σ)	Spatial resolution	Signal Quantization levels
VNIR	1	0.52-0.60	NEΔρ≤0.5%	≤ ± 4 %	15 m	8 bits
	2	0.63-0.69				
	3N	0.78-0.86				
	3B	0.78-0.86				
SWIR	4	1.600-1.700	NEΔρ≤0.5%			
	5	2.145-2.185	NEΔρ≤0.5%	≤ ± 4 %	3. m	8 bits
	6	2.185-2.225	NEΔρ≤0.5%			
	7	2.235-2.285	NEΔρ≤0.5%			
	8	2.295-2.365	NEΔT≤0.3K.	≤ 3 K (200-240 K)	90 m	12 bits
	9	2.360-2.430		≤ 2 K (240-270 K)		
TIR	10	8.125-8.475		≤ 1 K (270-340 K)		
	11	8.475-8.825		≤ 2 K (340-370 K)		
	12	8.925-9.275				
	13	10.25-10.95				
	14	10.95-11.65				
Stereo base-to-height ratio		0.6 (along-track)				
Swath width		60 km				
Total coverage in		232 km				
		Cross-track direction				
		By pointing				
Mission life		5 years				
MTF at Nyquist frequency		0.25 (cross-track)				
		0.20 (along-track)				
Band-to-band registration		Intra-telescope:0.2 pixels				
		Intra-telescope:0.3 pixels				
		of coarser band				
Peak data rate		89.2 Mbps				
Mass		406 kg				
Peak power		726 W				

Band number 3N refers to the nadir pointing view, whereas 3B designates the backward pointing view (modified from Rowan and Mars, [70],After Fujisada, [69]).

Table 2. Reflectance values of the dry and wet conditions of cyanobacteria extracted from Karnieli and Sarafis[24],

	VNIR bands		
Cyanobacteria	1	2	3
Dry conditions	0.31	0.33	0.36
Wet conditions	0.18	0.17	0.21

Table 3. Reflectance values of the hematite and magnetite-goethite extracted from Groove et al. [19].

	VNIR bands		
Iron minerals	1	2	3
Hematite	0.13	0.18	0.24
Magnetite-oethite	0.20	0.26	0.40

Table 4. Coordination and culturing results of cyanobacteria soil crust at Chadormalu desert area.

Sample code	culturing result	Coordination	Genus and Species
Cyb1	+	N32 21 1.71, E55 30 18.5	*Microcystis*
Cyb2	+	N32 19 56.42, E55 30 30.5	*M. vaginatous*
Cyb3	+	N32 19 57.5, E55 30 16.8	*Chroococcidiopsis*
Cyb4	+	N32 20 36.8, E55 29 28.7	*Nostoc. spp*
Cyb6	+	N32 22 12.1, E55 28 30.1	*Microcystis*
Cyb8	+	N32 21 23.4, E55 29 9.1	*M. vaginatous*
Cyb9	+	N32 21 49.6, E55 29 25.3	*Nostoc. spp*
Cyb10	-	N32 20 22.3, E55 29 13.9	-
Cyb12	+	N32 21 33.7, E55 28 13.0	very small, ND
Cyb13	+	N32 21 5.7, E55 28 8.1	*Nostoc. spp*
Cyb15	+	N32 17 55.1, E55 30 46.1	*Nostoc. spp*
Cyb19	-	N32 21 14.63, E55 30 59.2	-
Cyb20	-	N32 21 12.02, E55 31 50.6	-
Cyb18	-	N32 20 36.07, E55 31 55.6	-

A number of cyanobacteria release extracellular ferric specific chelating agents (*sidrophores*) during periods of low iron availability[54]. These agents function as extracellular ligands that aid in the solubilization and assimilation of Fe^{3+} to limit growth. In other words they are thought to function as a part of high affinity iron acquisitions systems similar to those found in other eubacteria and fungi[55,56]. This mechanism is resulted into that blue-green algae have an impressive ability to colonize in fertile substrates such as soils, sands and rocks[57,58,59]. Some researchers[60] added Fe as Fe-EDTA, EDTA-chelated and unchelated

Table 5. Coordination and XRD results of iron contamination at Chadormalu desert area, p = primary or geogenic contamination, s = secondary or anthropogenic contamination

Sample code	XRD result	Coordination	Mineral results
ST.1	+	N32 19 56.16, E55 30 32.2	*Mgn-hem-geot (p)*
ST.2mag	+	N32 20 33.40, E55 29 25.6	*Mgn-geot-hem (s)*
ST.2hem	+	N32 20 33.40, E55 29 25.6	*Hem- mgn-geot (s)*
ST.3	+	N32 20 48.8, E55 29 17.7	*Mgn-hem- geot (s)*
ST.3rock	+	N32 20 48.8, E55 29 17.7	*Mgn-hem-geot (s), (p)*
ST.5hem	+	N32 22 15.6, E55 28 35.00	*Mgn-hem-geot (s),(p)*
ST.5lim	+	N32 22 15.6, E55 28 35.00	*Geot (minor phase (s)*
ST.6	-	N32 22 12.08, E55 28 30.7	-
ST.6-21	-	N32 24 39.00, E55 29 53.5	-
ST.6-21sed	+	N32 24 44.8, E55 29 53.8	*Hem (p)*
ST.9	+	N32 20 2183, E55 32 26.35	*Hem-mgn-geot (s)*
ST.10	+	N32 22 12.00, E55 28 9.09	*Geot (minor phase)(p)*
ST.15	+	N32 21 58.80, E55 29 09.3	*Mgn (minor phase)(p)*
ST.17	+	N32 17 52.80, E55 30 57.6	*Mgn-hem-geot (s)*
T.18(1)	-	N32 21 58.30, E55 28 8.20	-
ST.19	+	N32 20 46.00, E55 29 32.9	*Mgn-hem-geot (s)*
ST. verny	+	N32 22 27.6, E55 29 28.80	*Mgn (minor phase)(p)*

$FeCl_3$ in both naturally occurring and cultured *Trichodesmium* populations and enhanced N_2-fixation (nitrogen activity), photosynthesis (CO_2- fixation), and growth (chlorophyll *a* production). According to Silva and Silva[61] Fe addition as $FeCl_3$ and Fe Na-EDTA salts increase biomass concentration sharply. Wells *et al.*[62] suggested that phytoplankton may utilize a variety of strategies for extracting iron from the surrounding environments, including: a) uptake of Fe by membrane bound porter sites b) uptake of Fe- sidrophore chelates c) extracellular reduction d) excess uptake and storage, and e) solid phase Fe acquisition (e.g. Chadormalu desert).

The extent of cyanobacterial blooms has been mapped using different satellite sensors[63,64]. Gones *et al.*[63] used one of the first satellite sensors, MERIS (satellite-based digital imagining spectrometers with a less than 1-km spatial resolution and suitable spectral band width) that can be applied to map cyanobacterial distributions in inland waters (*i. e*. Lake Ijsselmeer, Nederland). Based on retrieval algorithms to estimate phycocyanin, MERIS data can produce synoptic views of cyanobacterial bloom formation and dispersal.

Fig. 1a Published in B/W

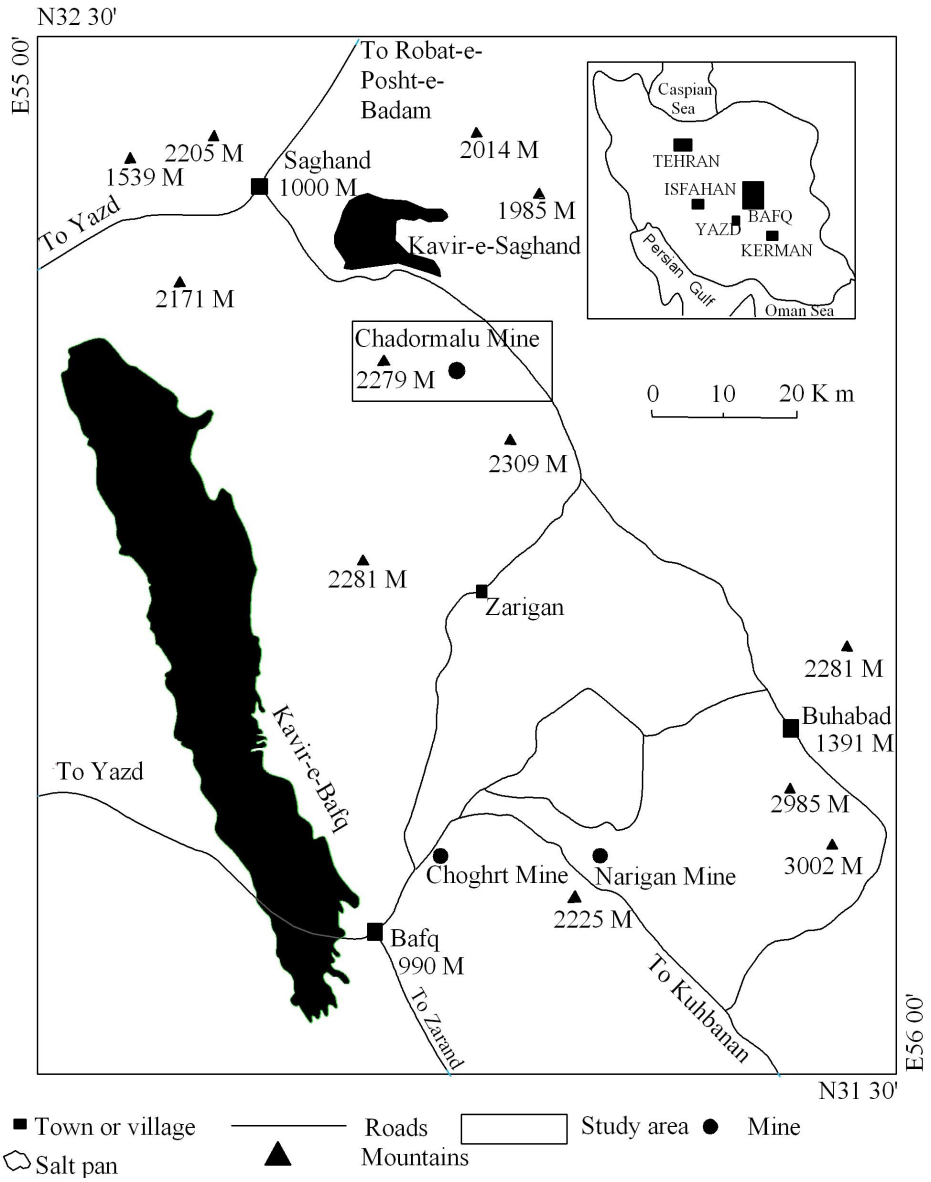

Fig.l. (a) Location of Chadormalu desert area in central Iran (b) Geological map of Chadormalu desert and Chadormalu iron oxide deposit (bordered area) (Modified from Moghtaderi[32] *et al*.).

Fig. 1b Published in B/W

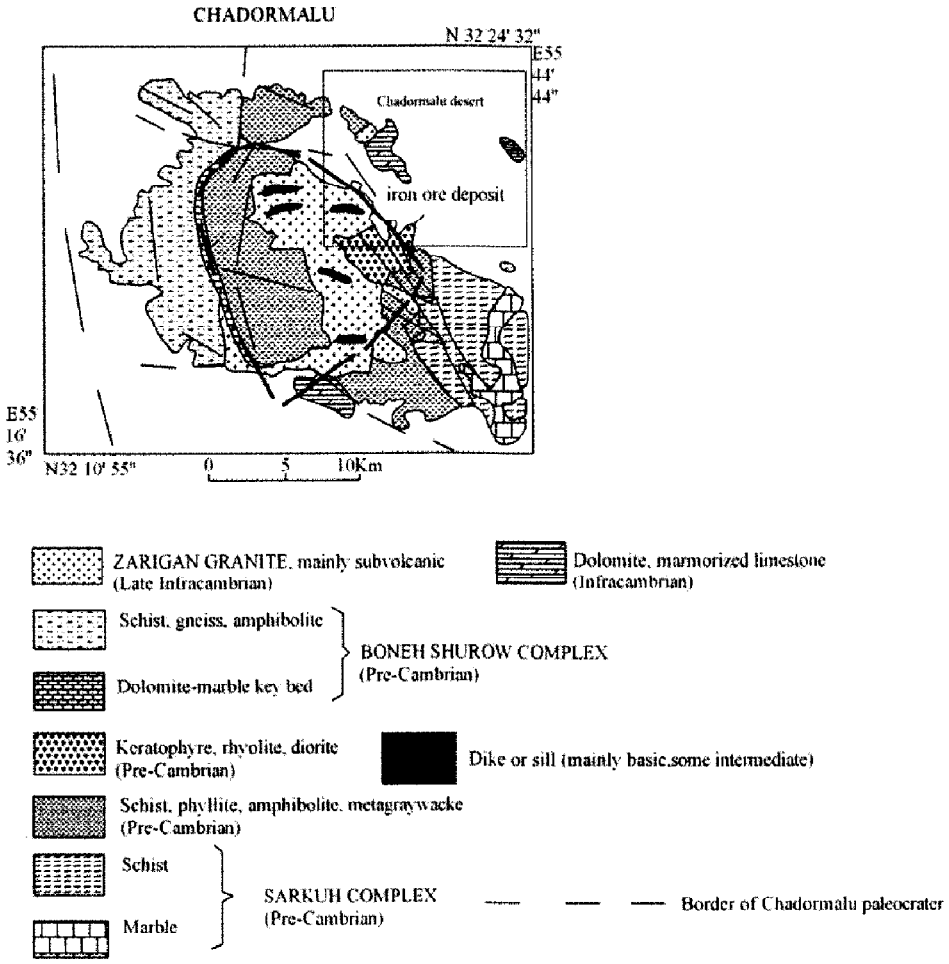

These authors suggested that airborne, spaceborne remote sensings and shipboard observation need to be exploited in concreted programmes of data acquisition, validation and reporting in summer time. The amount of chlorophyll-α is extremely variable spatially[65]. Simis *et al.*[64] have shown that their reflectance band-ratio algorithm for retrieval of cyanobacterial phycoyanin concentration (PC) decreased gradually with time in Lake Ijsselmeer throughout the period April–September (when cyanobacterial abundance is known to be high). Therefore, these studies did not capture the seasonal variability necessary for a more complete validation procedure[66].

Kutser *et al.*[67] show that MODIS band 1 response to changes in the concentration of cyanobacteria is nonlinear. Band 1 response is strongest in the case of *Nodularia spumigena*,

Fig 2
Published in B/W

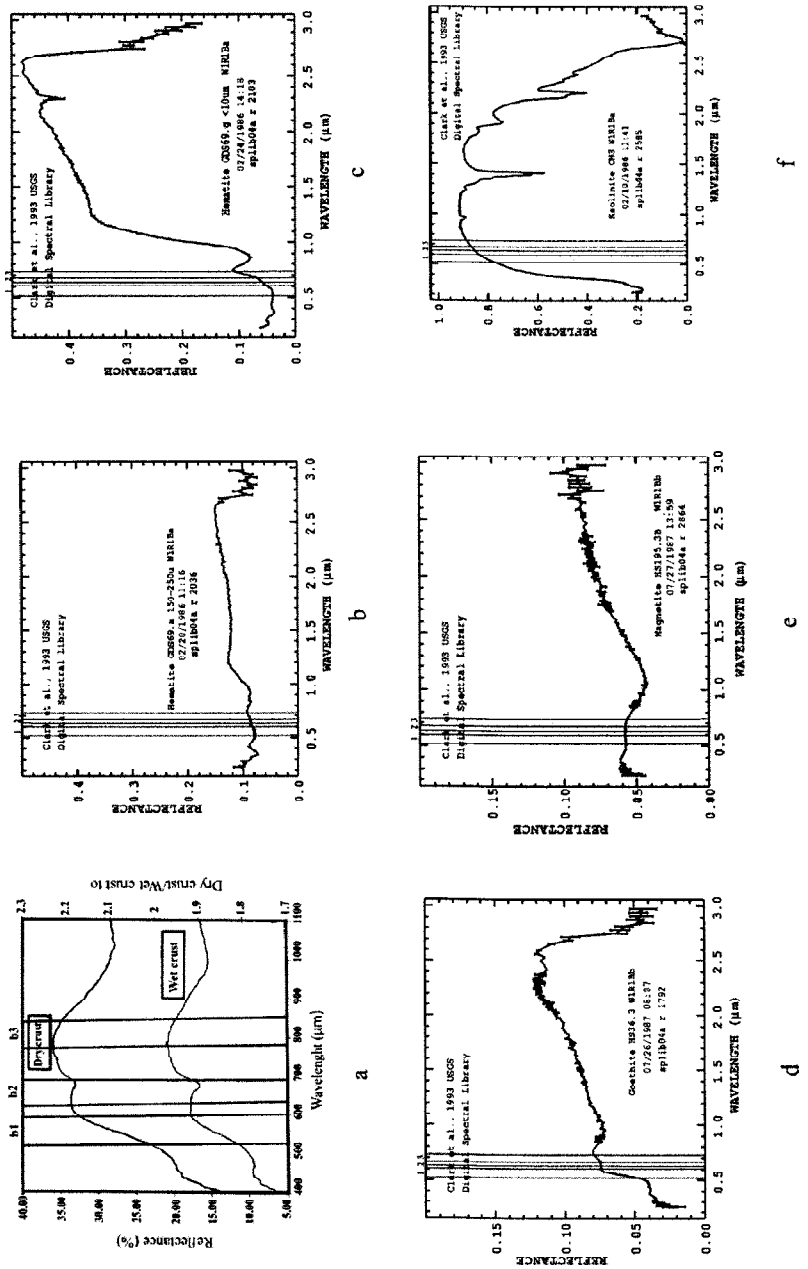

Fig 2 (a) Spectral reflectance curve of Cyanobacteria in dry and wet conditions (Modified from Karnieli and Sarafis[19]) (nm = Nanometer) compared with clay and Iron minerals

Published in B/W

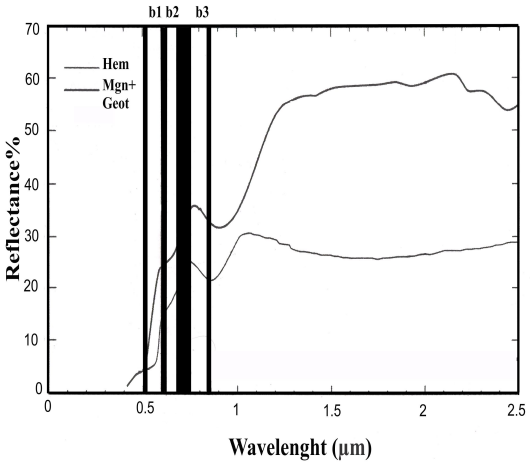

Fig. 3. (a, b) Spectral reflectance curves of hematite and magnetite-goethite (Modified from Groove[19] *et al.*; Singer[43]).

Published in B/W

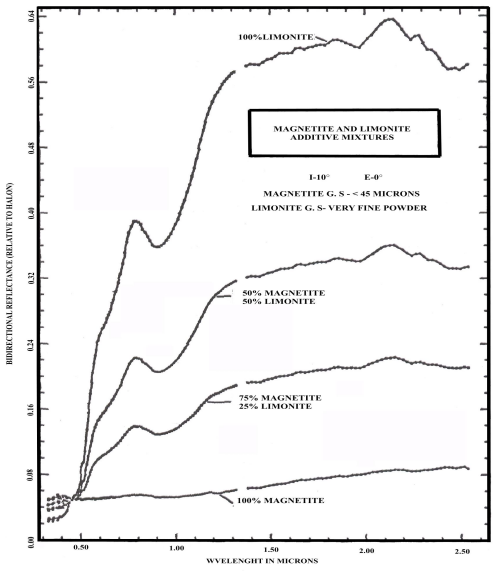

(Fig. 3b-f) including the Hematite, goethite, magnetite, and kaolinite respectively, in each figure, there is not any overlap between Fig. 3 a and spectral reflectance curves of clay and iron minerals especially in dry condition.

Published in B/W

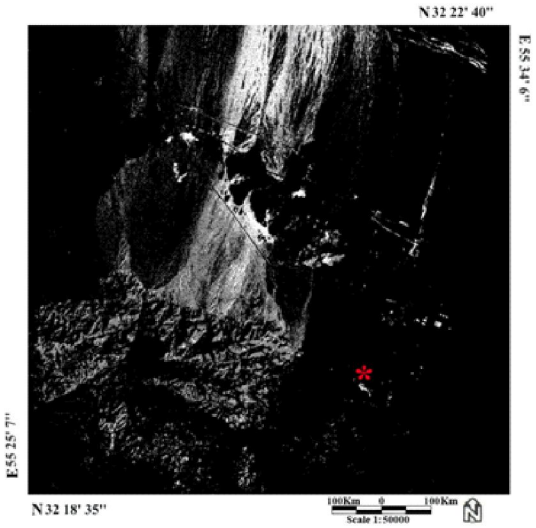

Fig. 4. (a) Detected cyanobacteria soil crust (MEM 3 2 1) in Chadormalu desert and iron mine (* area), (b, c) Detected hematite and magnetite-goethite contaminations (MEM 3 2 1) in Chadormalu desert and iron mine area (ST 17), respectively.

Fig. 4b

Published in B/W

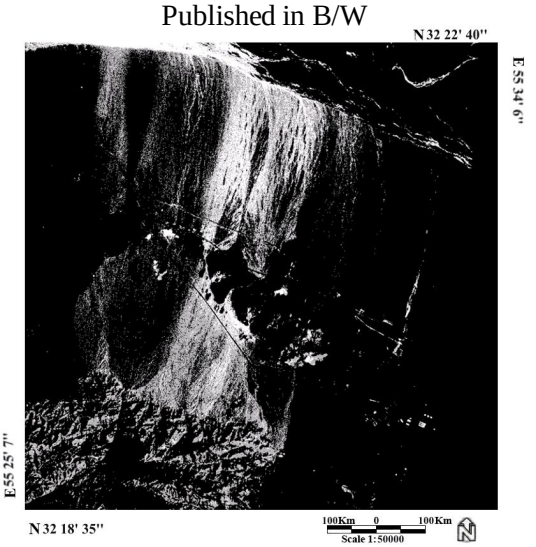

Published in B/W

Fig. 4c

Published in color (pdf file only or color on web only)

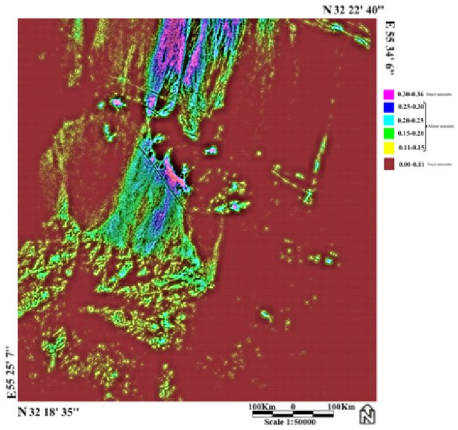

Fig. 5 (a) MEM321 pseudo color display, dark and pale pink colors correspond to major amounts (DN= 0.3-0.36) of the microorganisms, while, green, yellow, cyan, and blue colors represent minor amounts (DN=0.11-0.30) and trace amounts (DN= 0.00-0.11) are represented in dark red color, (b, c) MEM321 pseudo color displays, dark and pale pink colors correspond to major amounts of the hematite (b) and magnetite-goethite (c) , while, green, yellow, cyan, and blue colors represent minor amounts and trace amounts are represented in dark red color, d and e) Soil sampling stations at Chadormalu desert for Cyanobacteria (d) and iron minerals (e). Each sampling station is shown by dark red spot.

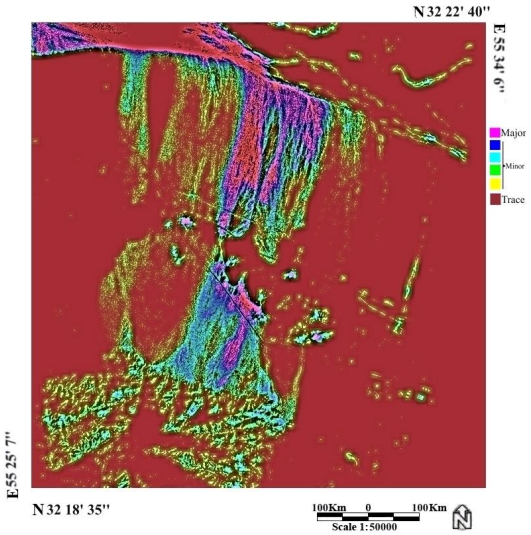

Fig. 5b
Published in color (pdf file only or color on web only)

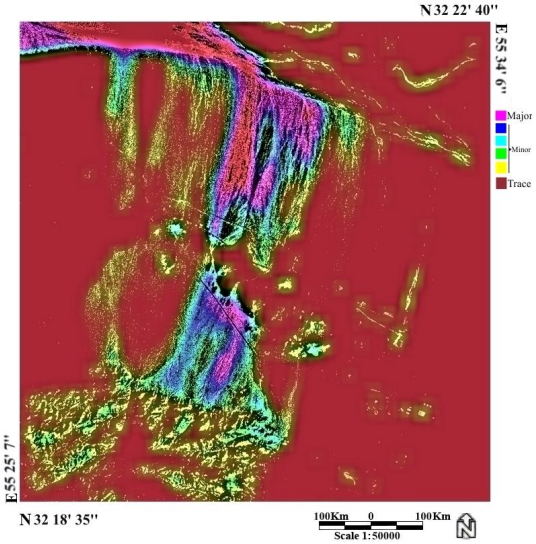

Fig. 5c
Published in color (pdf file only or color on web only)

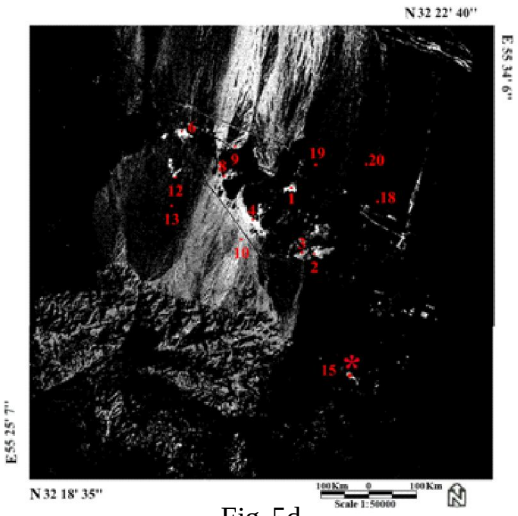

Fig. 5d
Published in B/W

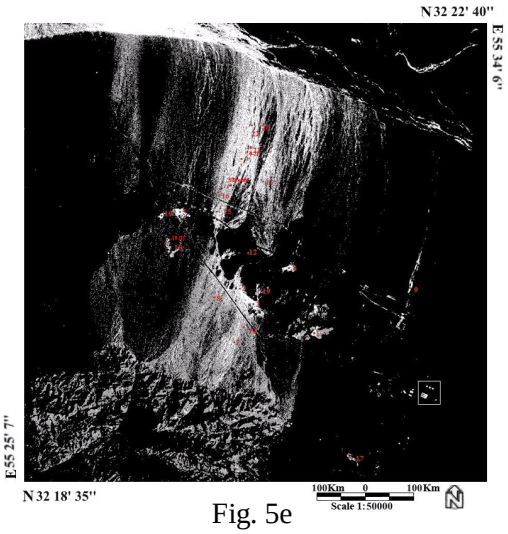

Fig. 5e
Published in B/W

Fig. 6. (pdf file only or color on web only)

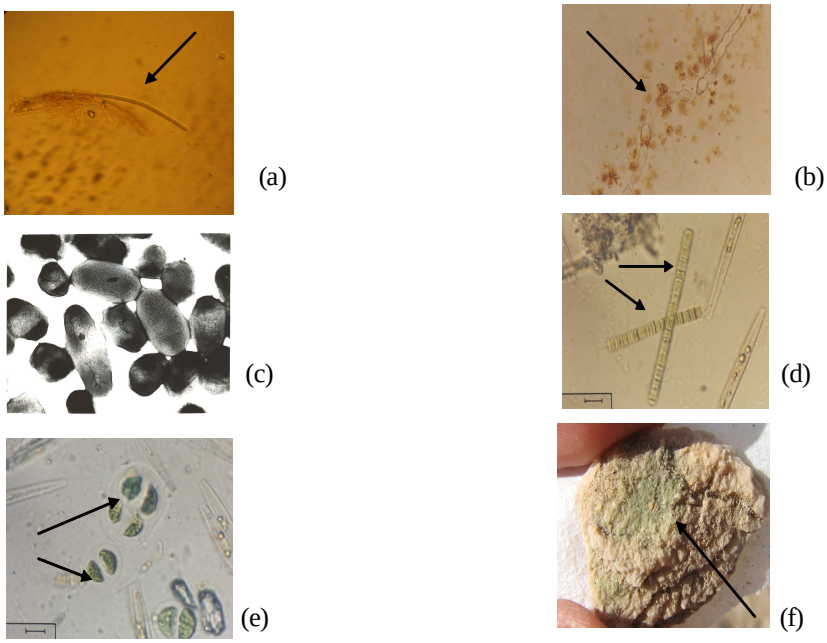

Fig. 6 (a) Microcoleous vaginatus in 4x (b) a Nostoc filamentous with l0x (phase microscope (c) Microcystis colony under TEM (28000x). TEM= Transmitted Electron Microscope (d) Ocillatoria.spp filamentous (40x) were prepared by phase microscope, (e) unicellular Chroococcuss.spp (40x, phase microscope), (f) Endolithic cyanobacteria (Chroococcidiopsis).

Fig. 7. (pdf file only or color on web only)

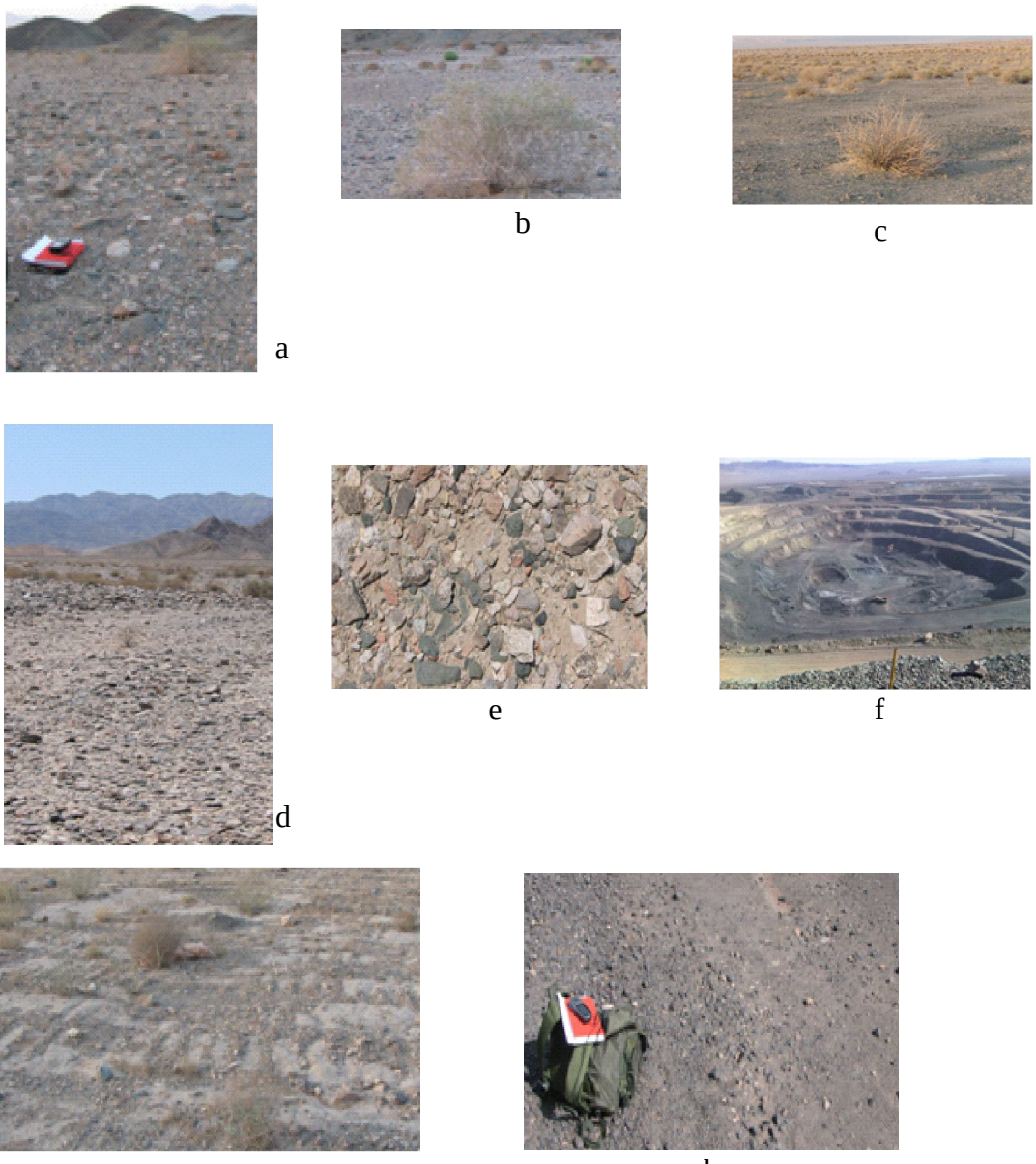

Fig. 7 (a, b) Rich soil area in Cybl soil sampling station with high vegetation cover (c) Rich soil area in Cyb9 soil sampling station with higher vegetation cover than Cybl (d, e) Barren area at Cybl9 soil sampling station (f) mining activity at Chadormalu iron deposit (g) motorized vehicles activity at Chadormalu iron deposit.

Fig. 8. (pdf file only or color on web only)

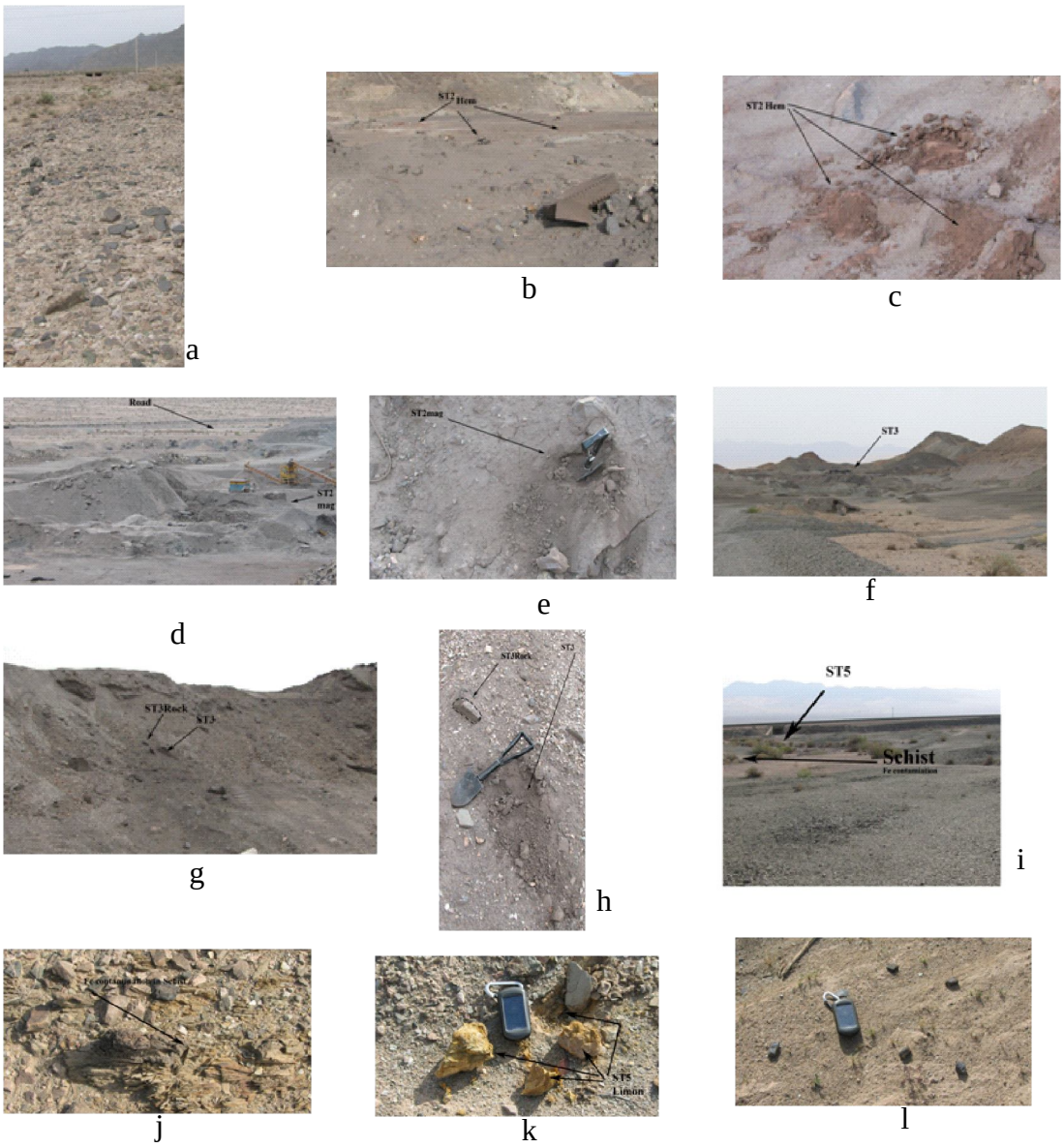

Fig. 8. (a) Iron mineral fragments in sampling station no. 1 (Ref to Fig. 10a). (b, c) red hematite clay size in ST. 2 (Fig. 10b). (d, e) magnetite-goethite in ST. 2 (Fig. 10c) anthropogenic activities can be seen in Fig. 8d. (f-h) anthropogenic activities in ST. 3 (Fig. l0d, e). (i-o) hematitic schist, (j) Goethite fragments, (k) Iron metallurgical pollutions. (1, m) and stratiform iron bed in alluvial deposit, (n, o) in ST. 5 (Fig. l0f, g). (p) Full scope view landscape in ST. 6 (Fig. l0h) (q) ST 6-21 alluvial deposit with no white pixels (Fig. l0l-i). (r) Red hematite contamination in alluvial deposits (ST. 6-21sed) (Fig. l0j). (s-u) Hematite-magnetite- goethite pebble in ST.9 (Fig. 10k). (v-x) Hematitic schist in ST.10 (Fig. 101). (y) Magnetite fragments in ST.15 (Fig. 10m).

Fig. 8. (continue) (pdf file only or color on web only)


m

n

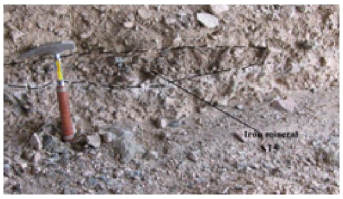

o

p


q

r

s

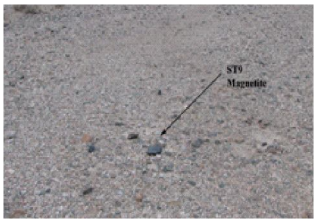

t

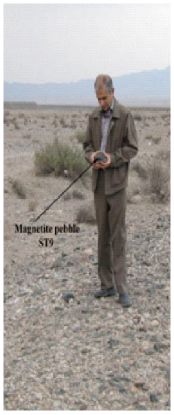

u

v

w

x

y

Fig. 9. (pdf file only or color on web only)

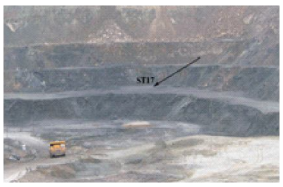

a

b

c

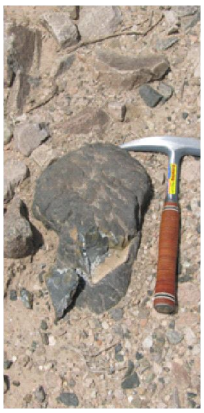

d

e

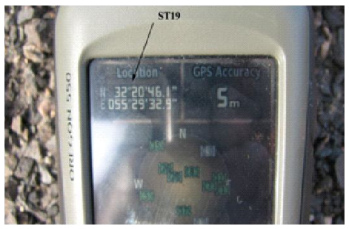

f

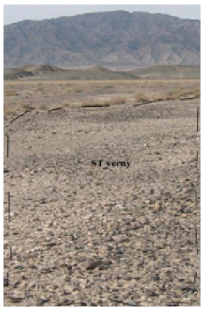

g

h

i

j

Fig. 9. (a) Iron mining floor at Chadormalu deposit (ST. 17). (b) magnetite-goethite (<45µm) at ST. 17 (Fig. l0n). (c, d) a landscape from ST. 18(1) (Fig. l0o), gray scale pixels, (e, f) anthropogenic activity in ST. 19 and its coordination (Fig. l0p). (g, h) ST. verny (Fig. l0q). (i, j) iron mineral dusts and iron concentration at ore processing factory.

Fig. 10. (Publish in B/W)

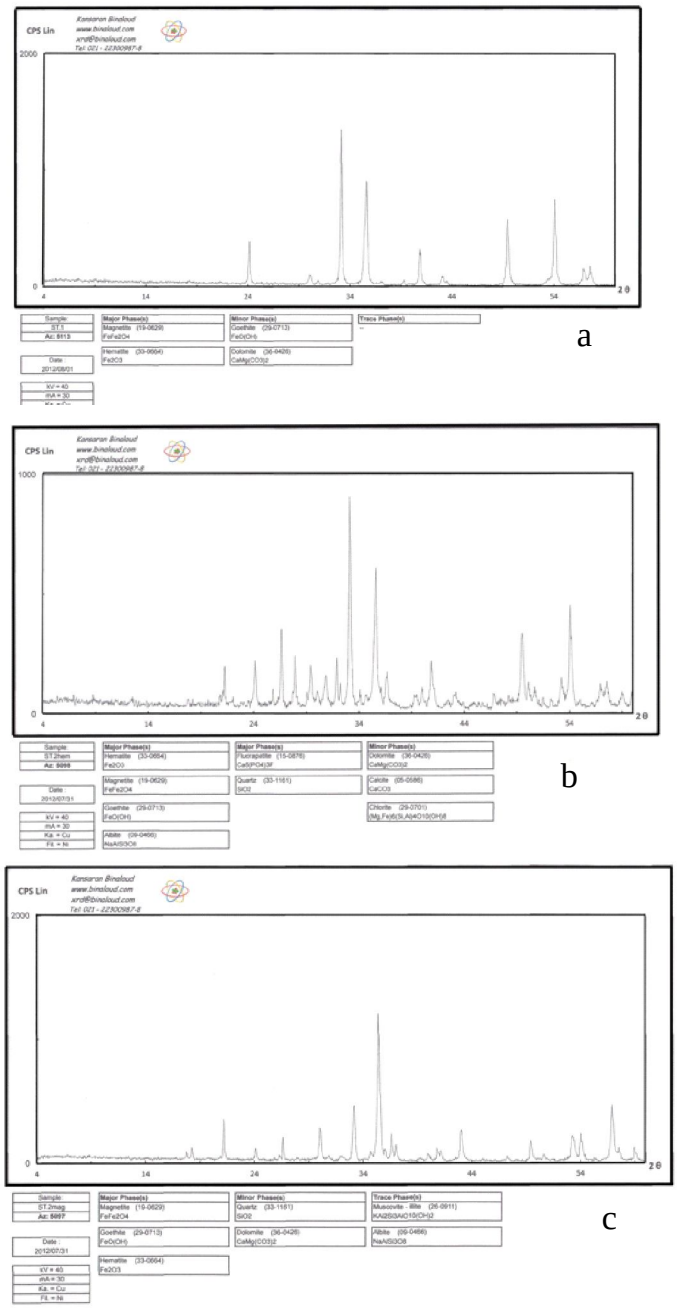

Fig. 10. X-ray diffraction diagram of Hematite, magnetite and goethite at sampling stations 1-17 and ST verny in major, minor and trace phases.

Fig. 10. (continue) (Publish in B/W)

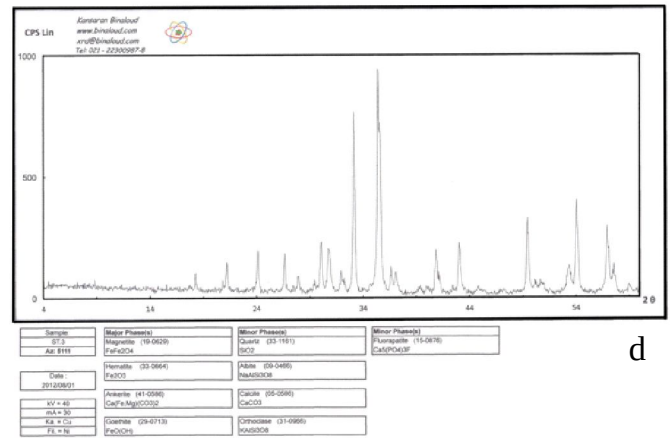

d

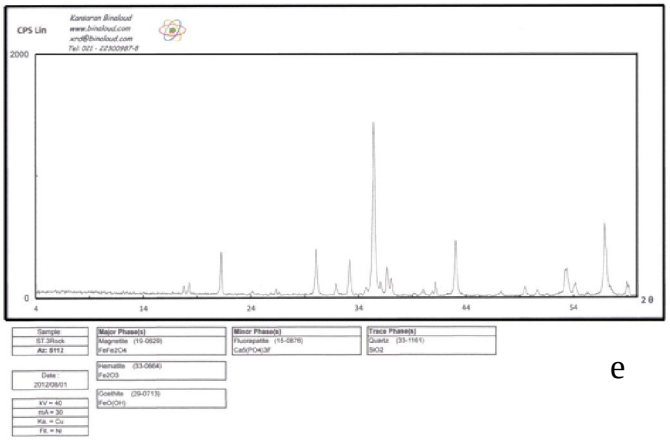

e

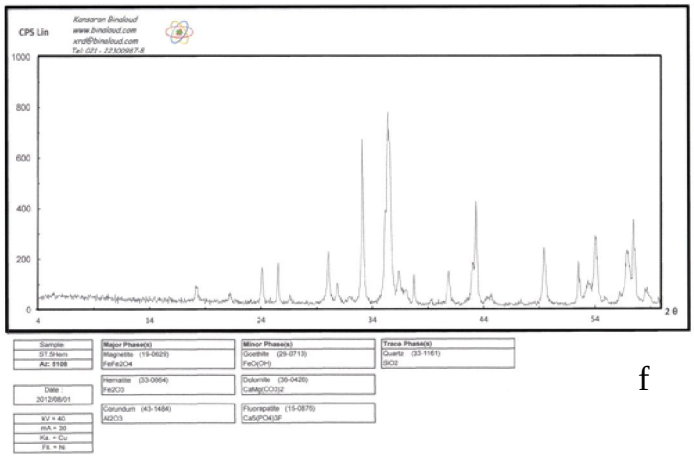

f

Fig. 10. (continue) (Publish in B/W)

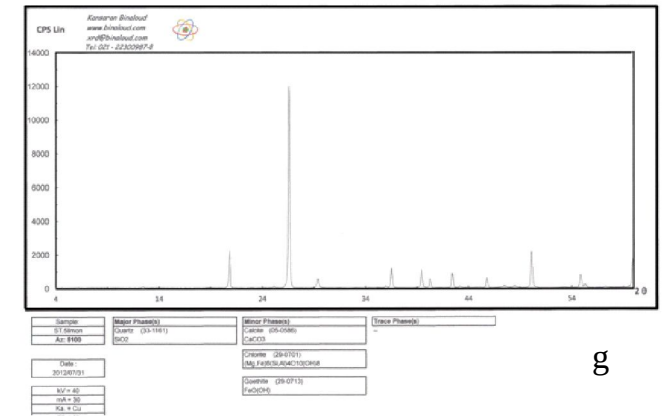

g

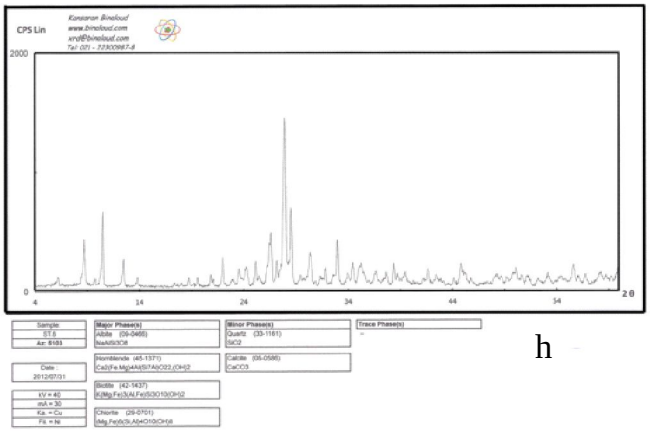

h

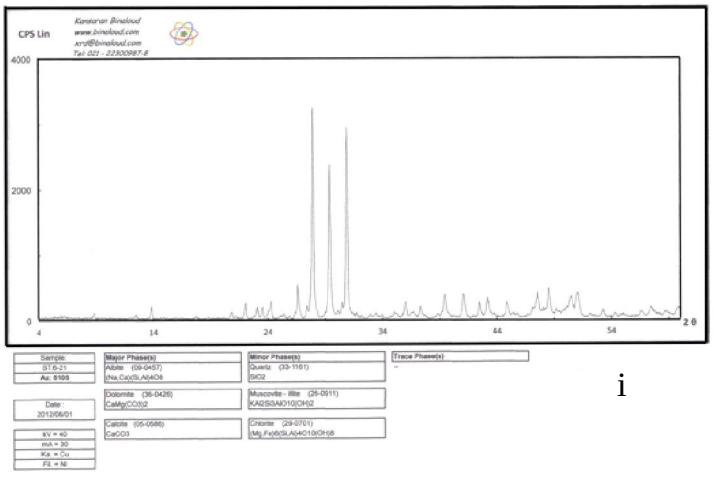

i

Fig. 10. (continue) (Publish in B/W)

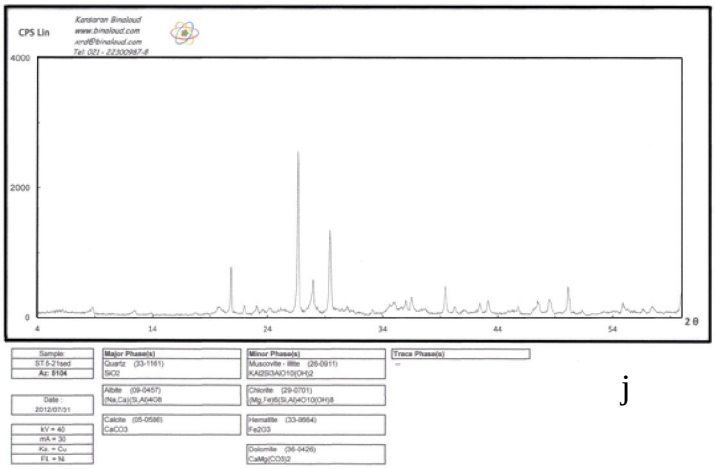

j

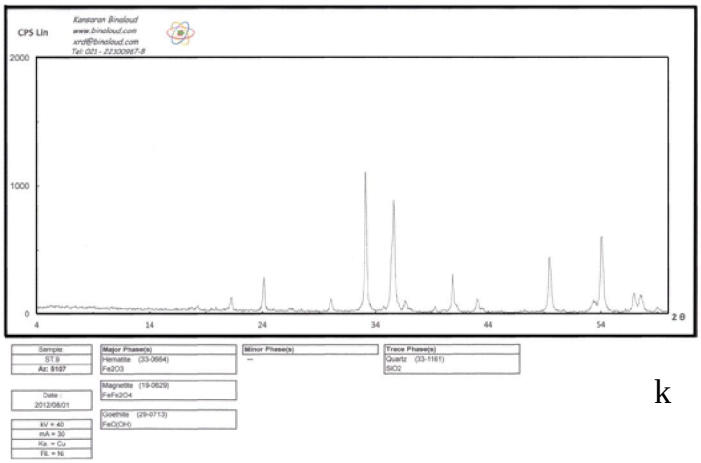

k

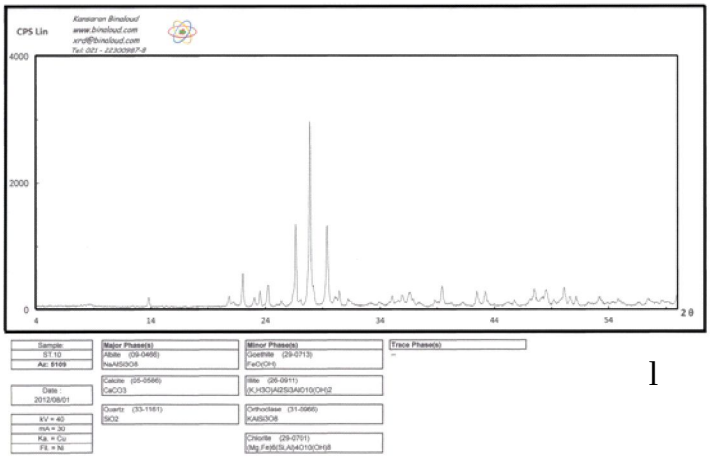

l

Fig. 10. (continue) (Publish in B/W)

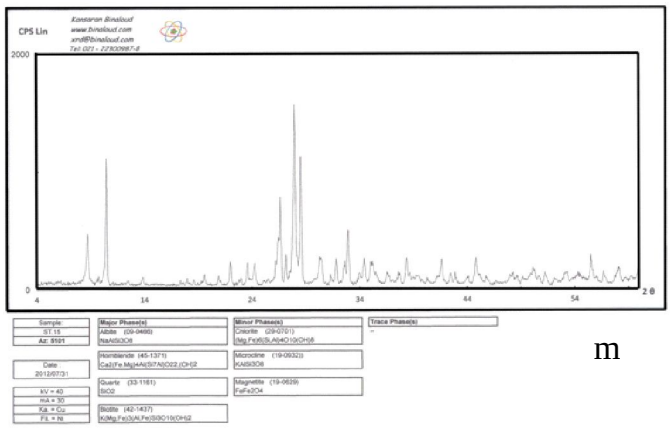

m

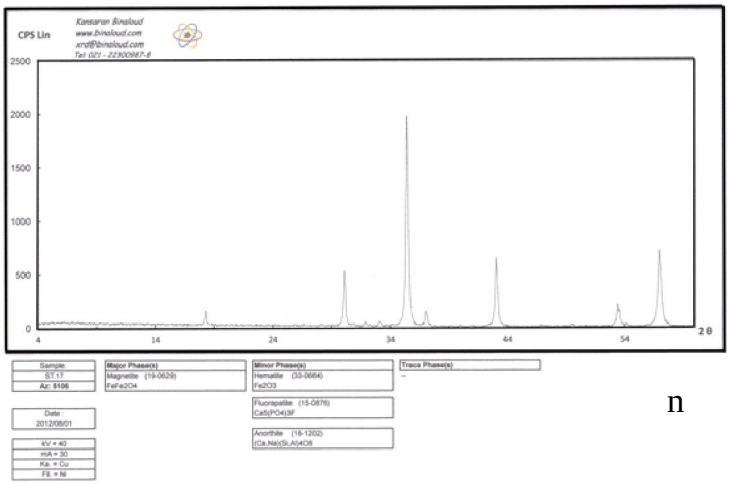

n

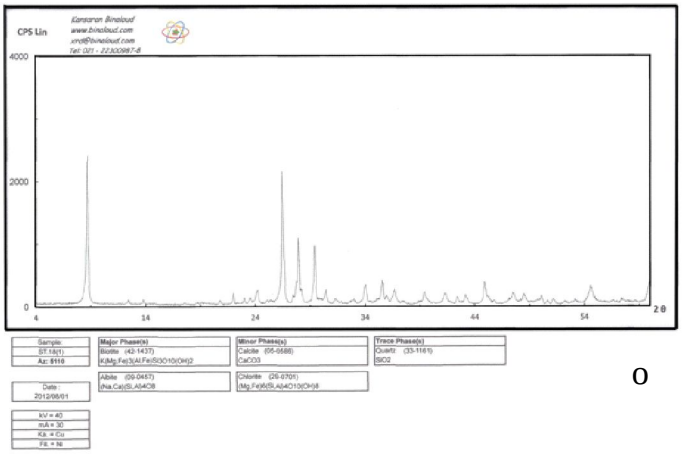

o

Fig. 10. (continue) (Publish in B/W)

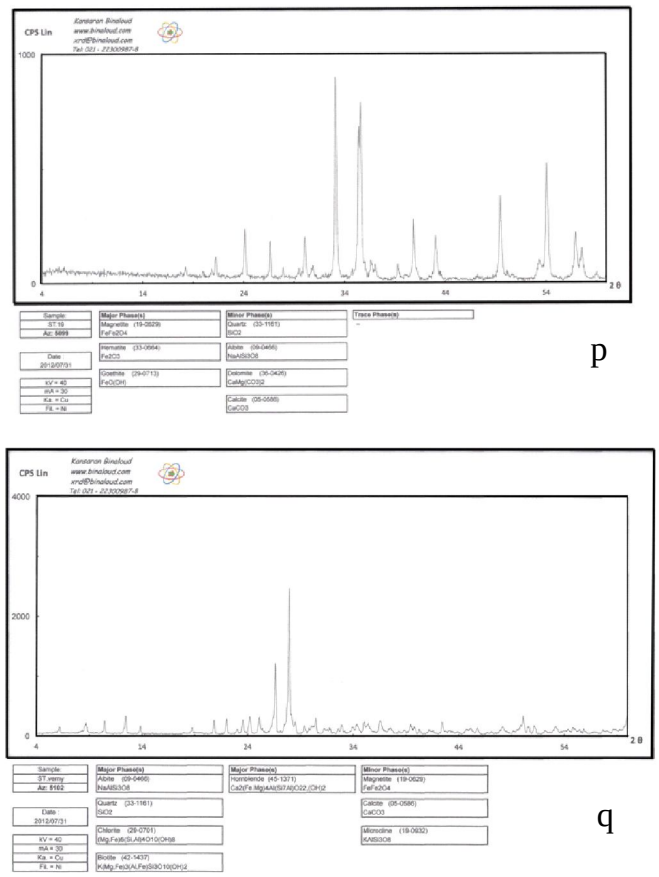

indicating that quantitative mapping of this species in bloom conditions is easier than in the case of the other species of cyanobacteria investigated. However, these researchers infer that quantitative mapping of cyanobacteria may be impossible by remote sensing sensors due to opaqueness of the scum and variability in the properties of cyanobacteria within the scum.

According to Kutser[68] quantitative detection of chlorophyll in cyanobacterial blooms by remote sensing has been less successful. Also, the chlorophyll estimation accuracy in cyanobacterial blooms by many satellites is limited because of spatial resolution, as significant changes in chlorophyll concentration occur even at a smaller spatial scale than 30 m (e.g. ALI, ASTER and Hyperion). In other words, the chlorophyll estimation accuracy in cyanobacterial blooms by remote sensing satellites (e.g. SeaWiFS, MERIS and MODIS) is limited as a result of their coarse spatial resolution and the fine spatial phenomena present in a bloom. The real chlorophyll values in dense cyanobacterial blooms can only be

estimated from remote sensing data. This, however, requires detailed knowledge about optical properties of the bloom, knowledge that is currently not available[69].

In this research, for the first time, a mathematical evaluation method was applied on the ASTER imagery data of a solid environment (Chadormalu desert soil), in dry or extreme conditions. Also, it must be noticed that ASTER bands (3, 2, 1 bands) have a higher spatial resolution (15m) than sensors used in the previous work. On the other hand, as already mentioned above MEM method is a relative estimation with a full scope view. However considering instrumental analysis limitation, especially the lack of a portable spectrometer, the obtained results must be considered approximations at their best. Despite this disadvantage, the proposed method is a fast technique that takes little time, is comparatively cheap, and suitable for reconnaissance stages[10].

This research demonstrates cyanobacteria growth –iron contamination relationships by remote sensing techniques at the Chadormalu desert. In other words, this study illustrates directional relationship of spatial distribution between cyanobacteria soil crust and major iron ores contamination at this mining area, probably related to cyanobacteria physiology. Furthermore, it demonstrated remote sensing ability in detecting relations between cyanobacteria soil crust area size and heavy metal (*i.e*. iron) contamination extension. The above proposed MEM method, despite being approximate is suitable in detecting iron contamination in inaccessible remote areas on earth or may be useful in astrobiological studies, especially, in Mars biological explorations.

Acknowledgements

The authors wish to thank all members of Chadormalu min managing board for supporting this research. Thanks are also extended to Dr. Bob Agar, director of AGARSS Pty. Ltd. Australia, for providing the ASTER imageries.

References

1. W. Xing, G. Liu, Iron biogeochemistry and its environmental impacts in freshwater lakes, Fres. *Environ. Bulletin. 20*, 1339-1345 (2011).
2. F. Archibald, Lactobacillus plantarum, an organism not requiring iron, FEMS *Microbiol. Lett. 19*, 29-32 (1983).
3. J.E. Posey, F.C. Gherardini, Lack of a role for iron in the Lyme disease pathogen. Science. *288*, 1651-1653 (2000).
4. E.A. Webb, J.W. Moffett, J.B. Waterbury, Iron Stress in Open-Ocean Cyanobacteria *(Synechococcus, Trichodesmium,* and *Crocosphaera* spp.): Identification of the IdiA Protein, *Appl. Environ. Microbial. 67*, 5444-5452 (2001).
5. A. Kosakowska, M. Nedzi, J. Pempkowiak., Responses of the toxic cyanobacterium Microcystis aeruginosa to iron and humic substances, *Plant. Physio. Biochem. 45*, 365-370 (2007).
6. A.B. El-Sayed, M.M. El Fouly, S.M. Ghazy, N.A. El Semary, M.A. Hassoub, Some growth metabolites of two cyanobacteria species as affected by mineral nutrition, *Nat. Sci. 8*, 20-28 (2010).
7. S.W. Wilhelm, D.P. Maxwell, C.G. Trick, Growth iron requirements, and siderophore production in iron-limited S'nechococczks PCC 7002, Limnol. *Oceanogr. 41*, 89-97

(1996).
8. W.R. Odom, R. Hodges, P.R. Chitnis, J.A. Guikema, Characterization of Synechocystis sp. PCC 6803 in iron-supplied and iron-deficient media, *Plant Mol. Biol. 23,* 1255-1264 (1993).
9. L.P. Hardie, D.L. Balkwill, S. E. Stevens, JR, Effects of iron starvation on the physiology of the cyanobacterium Agmenellum quadruplicatum. *Appl. Environ. Microbial. 45,* 999-1006 (1983).
10. I. Berman-Frank, A.Q, Zoe, V. Finkel, A.J. Irwin, L. Haramaty, Nitrogen-fixation strategies and Fe requirements in cyano-bacteria, *Limnol. Oceanogr. 52,* 2260-2269 (2007).
11. J. Belnap, S. Phillips, M. Duniway, R. Reynolds, Soil fertility in deserts: a review on the influence of biological soil crusts and the effect of soil surface disturbance on nutrient inputs ans losses, Desertification in the Third Millennium, In: A.S. Alsharhan, W.W. Wood, A.S. Goudie, A. Fowler and E.M. Abdellatif (Eds.), Swets & Zeitlinger Publishers, Lisse, The Netherlands, pp. 245-252 (2003).
12. N.E. West, Structure and function of microphytic soil crusts in wild land ecosystems of arid and semi-arid regions, *Advan. Ecolog. Resear. 20,* 197-223 (1990).
13. A. Danin, Plant adaptation in desert dunes, *Jour. Arid. Environ. 21,* 193-212 (1991).
14. L.M. Shield, F. Drouet, Distributions of terrestrial algae within the Nevada test site, *Ame. Jour. Bota. 48,* 547-554 (1962).
15. T. M. Zobeek, D. W. Fryrear, Chemical and physical characteristics of windblown sediments II. Chemical characteristics and total soil and nutrient discharge, Trans. *Ame. Soci. Agri. Eng. 29,* 1037-1041 (1986).
16. E. Verrecchia., A. Yair, G.J. Kidron, K. Verrecchia, Physical properties of the psammophile cryptogamic crust and their consequences to the water regime of sandy soils, north-western Negev Desert, Israel, *Jour. Arid. Environ. 29,* 427-437 (1995).
17. A. Moghtaderi, F. Moore, S. M. Taghavi, R. Rezaei, The application of ASTER imageries and mathematical evaluation method in detecting cyanobacteria in biological soil crust, Chadormalu area, central Iran, *Iran. Jour. Sci. Techno. 35,* 13-28 (2011).
18 R.N. Clark, G.A. Swayze, A. Gallagher, T.V.V. King, W.M. Calvin, The U.S. Geological Survey Digital Spectral Library: Version 1: 0.2 to 3.0 mm, U.S. Geological Survey, *Open File Report*. 93-592, pp. 1340 (1993).
19. C. I. Grove, S. J. Hook, E. D. Paylor II, Laboratory Reflectance spectra of 160 minerals, 0.4 to 2.5 micrometers., Jet propulsion Laboratory publication. Pasadena: California Institute of Technology (1992).
20. J.W. Salisbury, L.S. Walter, N. Vergo, D.M. D'Aria, Infrared (2.1-25 micrometers) Spectra of Minerals., Johns Hopkins University Press, (1991b).
21. C.M. Ager, N.M. Milton, Spectral reflectance of Lichens and their effects on the reflectance of rock substrates, *Geophysics. 52,* 898-906 (1987).
22. A. Karnieli, G. J. Kidron, C. Glaesser, E. Ben-Dor, Spectral characteristics of cyanobacteria soil crust in semiarid environment, *Rem. Sens. Environ. 69,* 67-75 (1999).
23. A.L. O'Neill, Reflectance spectra of microphytic soil crusts in semi-arid Australia,

Inter. Jour. Rem. Sens. *15*, 675-681 (1994).
24. A. Karnieli, V. Sarafis, Reflectance spectrometry of cyanobacteria within soil crusts a diagnostic Tool, *Inter. Jour. Rem. Sens. 17*, 1609-1615 (1996).
25. M. Tromp, Z. Steenis, Deriving sub-pixel soil characteristics in Northern Burkina Faso with spectral unmixing. In: R. Escadafal, M.A. Mulders, L. Thiombiano (Eds.), proceedings of the ISSS International Symposium (Working Group RS and DM) on Monitoring Soils in the Environment with Remote Sensing and GIS, 1995, *Ouagadougou, Burkina Faso,* pp. 269-284 (1996).
26. P. N. Zombre, F. Pallo, M.A. Mulders, Excursion to the Kaya region, Burkina Faso. In: R. Escadafal, M.A. Mulders, L. Thiombiano (Eds.), proceedings of the ISSS International Symposium (Working Group RS and DM) on Monitoring Soils in the Environment with Remote Sensing and GIS, 1995, *Ouagadougou, Burkina Faso,* 569-592 (1996).
27. X. Zhang, M. Pazner, Comparison of Lithologic Mapping with ASTER, Hyperion and ETM Data in the Southeastern Chocolate Mountains, USA, Photogram. *Eng. Rem. Sens. 73*, 555-561 (2007).
28. S. Rajendran, A. Thirunavukkarasu, G. Balamurugan, K. Shankar, Discrimination of iron ore deposits of granulite terrain of Southern Peninsular India using ASTER data, *Jour. Asia. Earth Scis. 41*, 99-106 (2011).
29. A. Kalinowski, S. Oliver, ASTER mineral index processing manual, Remote Sensing Applications, Geoscience Australia (2004).
30. K. Conradsen, O. Harpoth, Use of Landsat Multispectral Scanner Data for detection and reconnaissance mapping of iron oxide staining in mineral exploration, central east Greenland, *Econ. Geol. 79*, 1229-1244 (1984).
31. M.G. Abdelsalam, R.G. Stern, W.G. Berhane, Mapping gossans in arid regions with Landsat TM and SIR-C images: the Beddaho Alteration Zone in northern Eritrea, *Jour. Afri. Earth Scis. 30*, 903-916 (2000).
32. A. Moghtaderi, F. Moore, A. Mohammadzadeh, The application of advanced space borne Thermal Emission and Reflection Radiometer (ASTER) data in Alteration mapping of Chadormalu paleocrater, Bafq region, central Iran, *Jour. Asia. Earth Scis. 30*, 238-252 (2007).
33. A. Moghtaderi, F. Moore, A. Mohammadzadeh,, The application of advanced space borne Thermal Emission and Reflection Radiometer (ASTER) data in Alteration mapping of Chadormalu paleocrater, Bafq region, central Iran, In: 33rd *International Geological Congress Oslo*, Norway (2008), J. P. Derion (Ed.), published in Photo-Interpretation European Journal of Applied Remote Sensing N° 2009/2, 45, 2009, pp. 79-87, (2e trimestre 2009 EDITIONS ESKA, 12, rue du Quatre-Septembre, 75002 PARIS).
34. S.E. Campbell, J. Seeler, S. Golubic, Desert crust formation and soil stabilization, Arid Soil. *Res. Rehab. Jour* (New title: Arid Land Research and Management). *3*, 217-228 (1989).
35. E. Svab, A.N. Tyler, T. Preston, M. Presing, K. V. Baloch, Characterizing the spectral reflectance of algae in lake waters with high suspended sediment concentrations, *Inter. Jour. Rem. Sens. 26*, 919-928 (2005).
36. O.L. Lange, G.J. Kidron, B. Budel, A.

Meyer, E. Kilian, A. Abeliovich, Taxonomic composition and photosynthetic characteristics of the biologic soil crust' covering sand dunes in western Negev Desert, *Func. Ecol. 6*, 519-527 (1992).
37. P.M. Mather, Computer processing of remotely - sensed images, an introduction, John Wiley and Sons, Publisher, second Ed, New York, (1999).
38. G. Ferrier, K. White, G. Griffiths, R. Bryant, M. Stefouli, The mapping of hydrothermal alteration zones on the island of Lesvos, Greece, using an integrated remote sensing data set, *Inter. Jour. Rem. Sens. 23*, 341-356 (2002).
39. J. Belnap, Recovery rates of cryptobiotic crusts: inoculants use and assessment methods, *Great Basin National park 53*, 89-95 (1993).
40. A. Karnieli, Development and implementation of spectral crust index over dune sands, *Inter. Jour. Rem. Sens. 18*, 1207-1220 (1997).
41. G.R. Hunt, Spectral signatures of particulate minerals in the visible and near infrared, *Geophys. 42*, 501 - 513 (1977).
42. A.A. Green, J.F. Huntington, Remote sensing for surface mineralogy, In: Garland, G.D. (Ed.), Proceedings of Exploration'87:3rd Decennial International Conference on Geophysical and Geochemical Exploration for Minerals and Groundwater, pp. 213-228 (1989).
43. R.B. Singer, The composition of the Martian dark region: I. Visible and Near-Infrared spectral reflectance of analog materials and interpretation of telescopically observed spectral shape, NASA- CR-172753. Pub. No. 254, 1980, pp. 25.
44. R.K. Vincent, Fundamentals of geological and environmental remote sensing, Prentice Hall, (1997).
45. J. Belnap, Microbiotic crusts: their role in past and present ecosystems, *Park. Sci. 10*, 3-4 (1990b).
46. R.W. Castenholz, Culturing methods for cyanobacteria, *Meth. Enzymo. 167*, 68-93 (1988).
47. E.D. Hughes, R. Gorham, A. Zehnder, Toxicity of a unialgal culture of Microcystis aeruginosa, *Cana. Jour. Micro. 4*, 225-236 (1958).
48. M.M. Allen, Simple conditions for growth of unicellular blue-green algae on plates, *J. Phycol. 4*, 1-3 (1968).
49. R. Rippka, Isolation and Purification of cyanobacteria, *Meth. Enzymo. 167*, 3-27 (1988).
50. M. Shirai, K. Matumaru, A. Ohotake, Y. Takamura, T. Aida, M. Nakano, Development of a solid medium for growth and isolation of axenic Microcystis strains (Cyanobacteria). *Appl. Environ. Microbiol. 55*, 2569-2571 (1989).
51. J.B. Waterbury, The cyanobacteria-Isolation, Purification and Identification, In: M. Dworkin, S. Falkow, E. Rosenberg, K.H. Schleifer and E. Stackebrandt (Eds.), The prokaryotes, a handbook on biology of bacteria, Vol. 4, Springer., New York, pp. 1053-1073 (2006).
52. D. A. Hutchins, Iron and the marine phytoplankton community, *Prog. Phycol. Res. 11*, 1-48 (1995).
53. C.G. Trick., S. W. Wilhelm, Physiological changes in the coastal marine cyanobacterium Synechococcus sp. PCC 7002 exposed to low ferric ion levels, *Mar Chem. 50*, 207-217 (1995).
54. S.W. Wilhelm and C.G. Trick, Iron-limited growth of cyanobacteria: Multiple siderophore production is a common response, Limnol.

Oceanogr. 39, 1979-1 984 (1994).
55. C. G. Trick, A. Kerry, Isolation and purification of siderophores produced by cyanobacteria, Synechococcus (Anacystis nidulans R2) sp. and Anabaena variabilis, *Curr. Microbial. 24,* 241-245 (1992).
56. A. Kerry, D. L. Laudenbach, C. G. Trick, Influence of iron limitation and nitrogen source on growth and siderophore production by cyanobacteria, *J. Phycol. 24,* 566-571 (1988).
57. E.l. Friedmann, M. Galun, Desert algae, lichens, and fungi. In: G.W. Brown Jr (Ed.) Desert Biology, 2, Academic Press, New. York, pp. 165-212 (1974).
58. B. Metting, Biological surface features of semiarid lands and deserts. In: J. Skujins, (Ed) Semiarid lands and deserts: soil resource and reclamation. Marcel Dekkert, Inc., New York, pp. 257-293 (1991).
59. T.J. Painter, Carbohydrate polymers in desert reclamation—the potential of microalgal biofertilizers. *Carbohyd. Polym. 20,* 77-86 (1993).
60. H.W. Paerl, L. E. Prufert-Bebout, C. Guo, Iron-stimulated N2 fixation and growth in natural and cultured populations of the planktonic marine cyanobacterium Trichodesmium spp. *Appl. Environ. Microbiol. 60,* 1044-1047 (1994).
61. P.G. Silva, H.J. Silva, Effect of mineral nutrients on cell growth and self-flocculation of Tolypothrix tenuis for the production of a bio fertilizer, *Biores. Techno. 98,* 607-611 (2007).
62. M.L. Well, N. M. Priceb, K.W. Bruland, Iron chemistry in seawater and its relationship to phytoplankton: a workshop report, *Mar. Chem. 48,* 157-182 (1995).
63. H.J. Gons, H. Hakvoort, S.W.M. Peters, S.G.H. Simis, Optical detection of cyano-bacterial Blooms, shipboard observation and remote sensing, In: J. Huisman, H.C.P. Matthijs, P.M. Visser, (Eds.), Harmful Cyanobacteria, Springer, Netherland, 177-199 (2005).
64. S.G.H. Simis, S.W.M. Peters, H.J. Gons, Remote sensing of the cyanobacterial pigment phycocyanin in turbid inland water, *Limno. Ocean. 50,* 237-245 (2005).
65. L. Metsama, T. Kutser, On Suitability of MODIS Satellite Chlorophyll Products for the Baltic Sea Conditions, *Environ. Res. Eng. Manag. 44,* 4-9 (2008).
66. K. Randolph, J. Wilson, L. Tedesco, L. Li, D.L. Pascual, E. Soyeux, Hyperspectral remote sensing of cyanobacteria in turbid productive water using optically active pigments, chlorophyll a and phycocyanin, *Rem. Sens. Environ. 112,* 4009-4019 (2008).
67. L. Metsama, E. Vahtmae, N. Strombeck, Suitability of MODIS 250 m resolution band data for quantitative mapping of cyanobacterial blooms. In: A. Hillar, V. Kurnitsky (Eds.), Proceeding of the Estonian *Acad. Sci. Biol. Ecol,* 318-328 (2006).
68. T. Kutser, Quantitative detection of chlorophyll in cyanobacterial blooms by satellite remote sensing, *Limno. Ocean. 49,* 2179-2189 (2004).
69. H. Fujisada, Design and performance of ASTER instrument. In: J.B. Breckinridge, (Ed.), Proceedings of International Society for Optical Engineering, SPIE publication (AIP Online Journal Publishing Service and American Institute of Physics), Bellingham, Washington, 16-25 (1995).
70. L.C. Rowan, J. C. Mars, Lithologic mapping in the Mountain Pass, California area using Advanced space-borne Thermal Emission and Reflection Radiometer (ASTER) data, *Rem. Sens. Environ. 84,* 350-366 (2003).